IRDR Working Paper Series
Integrated Research on Disaster Risk

Tropical Cyclone Storm Surge-Based Flood Risk Assessment Under Combined Scenarios of High Tides and Sea-Level Rise: A Case Study of Hainan Island, China

Ziying Zhou
Saini Yang
Fuyu Hu
Bingrui Chen
Xianwu Shi
Xiaoyan Liu

IRDR
Integrated Research on Disaster Risk

doi:10.1029/2023EF004236

About the Series

This Working Paper Series is a new publication of Integrated Research on Disaster Risk (IRDR), following the decision of the IRDR Scientific Committee in April 2019 to act to 'Expand IRDR Network and Scientific Output' (No. 5 of the IRDR Action Plan 2018-2020).

IRDR is an international scientific programme under co-sponsorship of the International Science Council (ISC) and United Nations Office for Disaster Risk Reduction (UNISDR) and with support from China Association for Science and Technology (CAST) and Chinese Academy of Sciences (CAS). Started in 2010, the Programme has been pioneering in the promoting international and interdisciplinary studies on DRR and has made its contributions through scientific publication and policy papers as well as dialogue toward shaping international agenda in the understanding disaster risks, bridging science and policy gaps and promoting knowledge for actions, all required in the Sendai Framework for Disaster Risk Reduction 2015-2030 (SFDRR) and its top priorities. Over time, the scientific agenda of IRDR has attracted many international renowned expertise and institutions. IRDR community is now, institutionally speaking, characterized by its strong Scientific Committee and six thematic working groups, thirteen IRDR national committees (IRDR NCs) and one regional committee (IRDR RC), eighteen international centres of excellence (IRDR ICoEs), a group of some one hundred fifty Young Scientists (IRDR YS) and a broad partnership with national, regional and international institutions working for SFDRR.

This Working Paper Series is thus specially made to facilitate the dissemination of the work of IRDR NCs, ICoEs, YS and institutions and individual experts that IRDR considers relevant to its mission and research agenda, and of important values for much broader range of audience working in DRR domains. As one will notice, all working papers in this series has anchored their relevance and contributions of their work toward SFDRR, IRDR, SDGs and Paris Agreement on climate change. It is the hope of the authors of the working papers and IRDR that this working paper series will not only bring new knowledge, experience and information toward disaster risk reduction, but also helped build better coherence of DRR with the mainstream agenda of UN today toward inclusive, resilient and sustainable human societies.

Team of IRDR-IPO

Tropical Cyclone Storm Surge-Based Flood Risk Assessment Under Combined Scenarios of High Tides and Sea-Level Rise: A Case Study of Hainan Island, China

Ziying Zhou[1,2,3],

Saini Yang[1,4],

Fuyu Hu[5,6*],

Bingrui Chen[7],

Xianwu Shi[8,9],

Xiaoyan Liu[8,9]

[1] Joint International Research Laboratory of Catastrophe Simulation and Systemic Risk Governance, Beijing Normal University, Zhuhai, China

[2] School of National Safety and Emergency Management, Beijing Normal University, Zhuhai, China

[3] School of Systems Science, Beijing Normal University, Beijing, China

[4] Integrated Research on Disaster Risk, Beijing, China

[5] School of International Affairs and Public Administration, Ocean University of China, Qingdao, China

[6] Key Laboratory of Coastal Science and Integrated Management, Ministry of Natural Resources, Qingdao, China

[7] East China Sea Forecasting and Hazard Mitigation Center, Ministry of Natural Resources, Shanghai, China

[8] Faculty of Geographical Science, Beijing Normal University, Beijing, China

[9] Key Laboratory of Environmental Change and Natural Disaster, Ministry of Education, Beijing Normal University, Beijing, China

* Corresponding Author: hufuyu@ouc.edu.cn

Published in 2024 by Integrated Research on Disaster Risk (IRDR), an interdisciplinary body of the International Science Council (ISC).

Cover photo: https://www.japantimes.co.jp/news/2024/09/07/asia-pacific/yagi-landfall-vietnam/

Design: Fang Lian

Edit: Ruiyi Zhu

Printed by IRDR

Printed in Beijing, China

Citation of this publication: Zhou, Z., Yang, S., Hu, F., Chen, B., Shi, X., & Liu, X. (2024). Tropical cyclone storm surge–based flood risk assessment under combined scenarios of high tides and sea–level rise: A case study of Hainan Island, China. *Earth's Future, 12,* e2023EF004236. https://doi.org/10.1029/2023EF004236

Acknowledgement: IRDR IPO appreciates the authors for contributing this paper to IRDR Working Paper Series.

Content

Abstract

In the context of climate change, coastal flood risk is intensifying globally, particularly in China, where intricate coastlines and frequent tropical cyclones make storm surges a major concern. Despite local government's efforts to initiate coastal monitoring networks and qualitative risk guidelines, there remains a gap in detailed and efficient quantitative assessments for combinations of multiple sea-level components. To address this, we develop the Tropical Cyclone Storm Surge-based Flood Risk Assessment under Combined Scenarios (TCSoS-FRACS). This framework integrates impacts of storm surges, high tides, and sea-level rise using a hybrid of statistical and dynamic models to balance reliability and efficiency. By combining hazard, exposure, and vulnerability, it incorporates economic and demographic factors for a deeper understanding of risk composition. Applying TCSoS-FRACS to Hainan Island reveals that the combined effects of storm surges, high tides, and sea-level rise significantly amplify local coastal flood risk, increasing economic losses to 4.27–5.90 times and affected populations to 4.96–6.23 times. Additionally, transitioning from Fossil-fueled Development (SSP5-8.5) to Sustainability (SSP1-1.9) can reduce the risk increase by approximately half. The equivalence in flood hazard between current high tides and future sea level under a sustainable scenario boosts confidence in climate change adaptation efforts. However, coastal cities with low hazard but high exposure need heightened vigilance in flood defense, as future risk could escalate sharply. Our study provides new insights into coastal flood risk on Hainan Island and other regions with similar profiles, offering a transferable and efficient tool for disaster risk management and aiding in regional sustainable development.

Key Points:

- Design a flood risk framework for TC storm surges combined with high tides and sea-level rise using hybrid dynamic and statistical models
- Equivalence in flood between current high tides and future sea level under a sustainable scenario boosts confidence in adaptation efforts
- Coastal cities with low hazard but high exposure need heightened vigilance in flood defense as future risk could dramatically escalate

Plain Language Summary

Climate change is intensifying coastal flood risk worldwide. We developed TCSoS-FRACS, a framework that assesses flood risk from storm surges, high tides, and sea-level rise, using a combination of dynamic and statistical models. This framework evaluates hazard, exposure, and vulnerability to predict affected populations and economic losses across various land uses. When applied to Hainan Island, it shows that the combination of storm surges, high tides, and rising sea levels significantly increases flood risk. However, transitioning from a Fossil-fueled Development Path to a Sustainability Path can reduce this increased risk almost by half. The study also finds that, on Hainan Island, current high tide hazards may be comparable to future sea-level rise hazards under a sustainable scenario, boosting confidence in adaptation efforts. Coastal cities with low hazard but high exposure need greater vigilance, as their future flood risk could rise sharply. Our research offers valuable insights and tools for managing coastal flood risk in Hainan Island and similar regions, supporting sustainable development and effective disaster management.

Main Text

1 Introduction

Storm surges induced by tropical cyclones (TCs), as a critical component of extreme coastal flooding, lead to significant economic losses and human casualties worldwide (Dullaart et al., 2021; Fang et al., 2014; Muis et al., 2016). From 1949 to 2016, global storm surge events resulted in direct economic losses amounting to 4951.85 billion USD (Jin et al., 2018). In recent years, with the progression of climate change, coastal flooding has notably increased in certain regions (Almar et al., 2021; Camus et al., 2021; Edmonds et al., 2020; Vousdoukas et al., 2018). On one hand, high-tide flooding triggered by astronomical tides alone has become more frequent in areas such as San Francisco (Sweet et al., 2018) and South China Sea (S. Li et al., 2023). On the other hand, tropical cyclones are found to be slowing down (Kossin, 2018) and rapidly intensifying as they approach coastal areas (Y. Li et al., 2023), increasing the likelihood of coinciding with astronomical high tides, which significantly amplifies the destructiveness of coastal flooding (Spicer et al., 2019). A prominent example is Hurricane Laura in 2020, which coincided with high tides in the Gulf Coast region of the United States, resulting in an estimated economic impact of over 19 billion USD (Greer et al., 2023; Pasch et al., 2021). Another example is Typhoon Kompasu in 2021, which hit the coast of Hainan, China, during high tides, causing sea levels to rise by up to 3 m and resulting in losses of 135.98 million CNY (Ministry of Natural Resources of the People's Republic of China, 2021).

Furthermore, sea-level rise caused by global warming presents new challenges for coastal areas through the permanent submergence of low-lying regions (Fox-Kemper et al., 2021; G. G. Garner, Kopp, et al., 2021; G. G. Garner, Hermans, et al., 2021; Kopp et al., 2019). Increasing evidence indicates that sea-level rise reduces the freeboard between high water levels and local flood thresholds, making even minor storm surges or tidal events more likely to cause coastal flooding (Ghanbari et al., 2019). While the traditional paradigm associates extreme sea levels with severe meteorological and oceanographic events (Hague et al., 2022), future sea-level rise may cause multiple non-extreme sea-level components to exceed higher thresholds and prolong event durations (S. Li et al., 2023; Serafin, Ruggiero, Parker, & Hill, 2019). Given this context, it is crucial to consider the combined contributions of storm surges, astronomical tides, and sea-level rise to coastal flooding under current and future scenarios. Such exploration is essential for promoting regional long-term sustainable development and achieving the goals outlined in the Sendai Framework for Disaster Risk Reduction 2015–2030 (UNDRR, 2015).

There are various coastal flood models that involve storm surges, including statistical models, machine learning models, and dynamic models. However, achieving a balance among reliability, efficiency, and practicality remains a complex challenge. (a) Statistical

models are based on tidal gauge records or climate reanalysis data and use extrapolation (Haigh & Wahl, 2019; Lowe et al., 2021) or regression (Camus et al., 2017; Tadesse et al., 2020) to decompose and predict different sea-level components. These models excel in computational efficiency and ease of implementation but rely heavily on long-term historical observations and often produce low-resolution results due to sparse observational coverage (Hamdi et al., 2023). (b) Machine learning models predict sea levels based on training with large data sets (Tadesse et al., 2020; Tiggeloven et al., 2021). They can explore complex, nonlinear relationships between sea-level components and meteorological factors. However, these relationships are often difficult to interpret due to the opacity of "black box" algorithms (Sonnewald et al., 2021). Insufficient data on extreme events often leads to underestimation in their predictions (Bruneau et al., 2020). (c) Dynamic models simulate the physical interactions between the atmosphere, ocean, and terrain to predict sealevel changes. Common dynamic storm surge models include the Sea, Lake, and Overland Surges from Hurricanes (SLOSH) model (Jelesnianski, 1992), the Advanced CIRCulation (ADCIRC) model (Luettich et al., 1992; Westerink et al., 1994), Delft3D (Roelvink & Van Banning, 1995) and MIKE21 (Warren & Bach, 1992). Although they are computationally intensive and time-consuming, they can fill gaps in regions lacking long-term observations and provide high-resolution predictions (Wood et al., 2023). Given the above, recent research has begun to focus on hybrid frameworks that combine dynamic models with statistical or machine learning models (Anderson et al., 2021; Serafin, Ruggiero, Parker, & Hill, 2019), which can capture peak water levels more accurately during extreme flood events while providing sufficient spatial details.

According to the framework proposed by the Intergovernmental Panel on Climate Change (IPCC), coastal flood risk can be delineated as the confluence of hazard, exposure, and vulnerability (Bilskie et al., 2022; Koks et al., 2015; S. Wang et al., 2021). Hazard encompasses the intensity, frequency, and associated drivers of floods, which can be measured by flood area (Miller & Shirzaei, 2021), flood depth (Hisamatsu et al., 2020) and coastal water levels (Serafin & Ruggiero, 2014). Exposure includes the entities at hazard from storm surges (Zhang et al., 2021), such as populations, properties, land uses, buildings, infrastructure, and more (Hauer et al., 2021; Neumann et al., 2015; Y. Wang et al., 2021). Vulnerability refers to the sensitivity to adverse flood impacts and is often quantified using fixed proxy indicators or variable depth-damage curves (Shi et al., 2020; S. Wang et al., 2021).

Initial explorations of storm surge-based flood risk, particularly under conditions of high tides and sea-level rise, has predominantly focused on the hazard dimension. While such unidimensional assessments can map the spatial patterns of storm surge hazards (Hisamatsu et al., 2020; Mori et al., 2021), assuming that exposed entities are uniformly distributed and respond similarly to hazards is unrealistic. Studies have shown that increased future risk from some extreme events is driven more by increased exposure in hazard-prone areas rather than by intensifying hazards (Knorr et al., 2016). In 2000, approximately 625 million people lived in low-lying coastal areas, with this number expected to reach 949 million by the 2030s and 1.4 billion by the 2060s (Neumann et al.,

2015). Moreover, given the growing concentration of populations and assets in urban areas and the clustering of cities along coastlines, rapid urbanization is further exacerbating flood risk (Kasmalkar et al., 2020). Therefore, a comprehensive storm surge flood risk assessment must integrate these fundamental hazard assessments with insights into how these hazards interact with exposed and vulnerable communities and assets.

Currently, flood risk assessments mainly include two approaches: indicator-based and economic loss-based assessments. Indicator-based assessments are qualitative methods that use a standardized set of indicators to represent different dimensions of risk (Ramirez et al., 2016; Rizzi et al., 2017; Sajjad et al., 2019; J. Wang, Yi, et al., 2018). These indicators are then aggregated through weighted summation or multiplication to obtain an overall risk score. This method is simple and easy to implement, and it is widely used in the current Chinese industry standard "Technical Directives for Risk Assessment and Zoning of Marine Disasters" (Ministry of Natural Resources of the People's Republic of China, 2019). However, it primarily offers a relative measure of risk, is sensitive to variations in data spatial resolution, and can be influenced by subjective factors during the weighting process. Economic loss - based assessments offer a quantitative approach to risk estimation through discrete loss values for specific scenarios (Ghanbari et al., 2019; Ha et al., 2022; Thomson et al., 2023; K. Wang et al., 2022) or through continuous loss curves based on probabilities (Iglesias et al., 2021; Rasmussen et al., 2020; Rozer et al., 2019). Compared to the former, economic loss - based assessments provide an objective measure of risk that can be compared across different regions, capturing more details about spatial variations in risk. Despite deep uncertainties surrounding future coastal flood risk (Rasmussen et al., 2020; Wong & Keller, 2017), such loss assessments help the public understand risk intuitively and provide effective references for government and community decision-making, especially in allocating maintenance and reconstruction funds and resources.

Despite extensive research on storm surge flood risk at global (Fang et al., 2014; Muis et al., 2016), national (Calafat et al., 2022; Fang et al., 2021; Jalili Pirani & Najafi, 2022) and regional scales (Bilskie et al., 2022; Eilander et al., 2023), there remains insufficient focus on developing island regions. Due to sea-level rise and increasing extreme weather events, these regions are experiencing disproportionately destructive consequences from climate change compared to their carbon emissions (Giardino et al., 2018; Vousdoukas et al., 2023). Against this backdrop, we chose Hainan Island, China, for our case study. It was motivated not only by its strategic position as China's free trade port linking Southeast and South Asia, but also for its potential implications for other regions with similar risk profiles. We developed TCSoS-FRACS, a comprehensive flood risk framework that combines TC storm surges with high tides and sea-level rise using hybrid dynamic and statistical models. This framework goes beyond hazard assessment alone, integrating economic and demographic factors to provide a deeper understanding of risk composition. It can serve as an efficient tool for disaster risk management across diverse geographic settings. Moreover, it contributes to the field by demonstrating how detailed,

integrated risk assessments can guide more effective policy-making and urban planning, particularly in developing island regions and similar environments.

2 Study Area and Data

2.1 Study Area

As shown in Figure 1, Hainan Island is located in the South China Sea (18°10'–20°10'N, 108°37'–111°03'E), bordered by the Qiongzhou Strait to the north and Beibu Bay to the west. Wuzhi Mountain, the highest point on the island, is situated centrally and surrounded by low-lying areas. The mixture of monsoonal and maritime climate commonly brings the island with strong rainfalls and TCs during the summer and autumn seasons. According to the Bulletin of China Marine Disaster, Hainan experienced 20 disastrous TC-induced storm surges between 2001 and 2020 (see Figure S1 in Supporting Information S1), causing total direct economic losses of over CNY 19.93 billion (details in Table S1 in Supporting Information S1). Among these, Typhoon Rammasun (TC-1409) alone caused CNY 2.73 billion in direct economic losses, accounting for 20.12% of the national total that year. Furthermore, the latest IPCC report (Fox-Kemper et al., 2021; G. G. Garner, Hermans, et al., 2021) projects that local sea levels will rise by 0.45 m (SSP1-1.9)–0.84 m (SSP5-8.5) from 2020 to 2100, further exacerbating the coastal flood risk on the island.

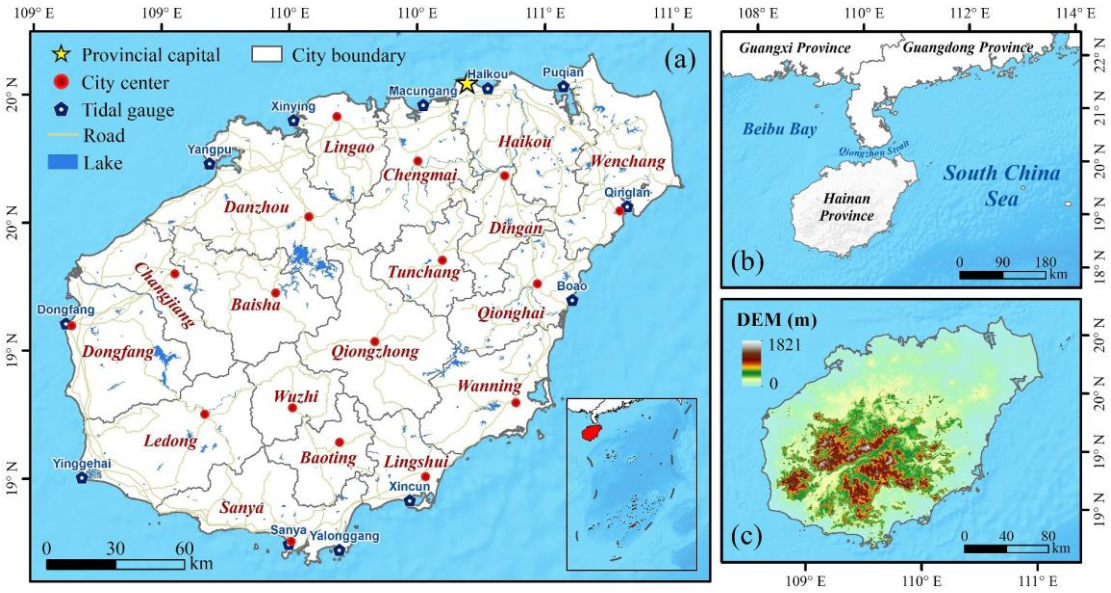

Fig 1 *Geographical location and topography of Hainan Island: (a) spatial distribution of basic geographical features; (b) geographical location of Hainan Island; and(c) digital elevation map of Hainan Island.*

2.2 Data

Multiple data sources were obtained and processed to evaluate the storm surge risk on Hainan Island, as shown in Table 1. Notably, the currency unit in the global flood damage database was converted from EUR in 2010 to USD in 2020 by using the EUR-USD exchange rate and the inflation rate before assessing economic losses. We set up a

reference time (2020 or 2100) to collect the corresponding data. However, due to data availability, we could only access bathymetry maps, and digital elevation maps from 2021. Fortunately, the natural elements represented by these data sets change slowly over a long time frame, so deviations within one or two years can be ignored reasonably.

3 Methods

3.1 Storm Surge Generation

In this section, we first constructed a local ADCIRC model for the interested region using bathymetry and DEM data, and input wind fields generated by the Fujita-Takahashi model (Fujita, 1952). Then, we validated the model reliability by comparing observed and simulated water levels during historical TC events. Finally, we performed extensive simulations based on synthetic TC tracks to estimate the annual exceedance probability for each mesh node, and obtained storm surge levels at 10-, 20-, 50-, and 100-year return periods.

3.1.1 Model Construction and Validation

The ADvanced CIRCulation (ADCIRC) model (Luettich et al., 1992; Westerink et al., 1994) is widely used incoastal flooding studies due to its accuracy and stability (Gori & Lin, 2022; Lockwood et al., 2022). It employs hydrostatic pressure and the finite element method to numerically solve shallow water equations and generalized wave continuity equations (details in Text S1 in Supporting Information S1). Here, we applied the ADCIRC model to generate local storm surges for Hainan Island, China. First, an unstructured mesh with 93,002 nodes and 183,264 elements was created for the geographical range of 105°–120° E, 10°–25°N, covering the majority of the South China Sea, Beibu Gulf, Qiongzhou Strait, and the coastal area of Hainan with elevation below 15 m (red lines in Figure S2 in Supporting Information S1). To balance efficiency and accuracy, element sizes were 30 km for offshore areas and 400 m for inshore areas, with bathymetry and DEM data interpolated by the Inverse Distance Weighting (IDW) method. Then, we utilized the Fujita-Takahashi model (Fujita, 1952) (details in Text S2 in Supporting Information S1), validated for the Northwest Pacific (Shi et al., 2021; Sun et al., 2015; Xu et al., 2020), to generate wind fields as meteorological forcing for the ADCIRC model. In addition, eight principal tidal constituents (M_2, S_2, N_2, K_2, K_1, O_1, P_1, Q_1) from the LeProvost Tidal Database (Le Provost et al., 1995) were set as the tidal inputs at the ocean boundary (blue lines in Figure S2 in Supporting Information S1).

Observations during *MUN* (TC-1904), *KAJIKI* (TC-1914), *Sinlaku* (TC-2003), and *Nanka* (TC-2016), from 12 tidal gauges along the coast of Hainan Island (see in Figure 1), were selected for validating the ADCIRC model. The simulated results of the highest and lowest water levels at each gauge were generally consistent with the actual values, and the phase differences were within 1 hour overall (Figures S3–S6 in Supporting Information S1). Specifically, the mean correlation coefficient was 0.90; the mean error of the maximum

Table 1

Data Sources and Descriptions

Data type	Time	Description	Source
Bathymetry map	2021	Resolution of 15 arc-seconds (≈450 m)	General Bathymetric Chart of the Oceans (GEBCO; Weatherall et al., 2021)
Digital elevation map	2021	Resolution of 90 m	Shuttle Radar Topography Mission Version 4 (SRTM V4; Jarvis et al., 2008)
Historical tidal observations	2018–2022	Hourly observations from local tidal gauges (details in Table S2 in Supporting Information S1), adjusted to mean sea level and UTC-0	China National Marine Data Center
Historical TC tracks	1949–2022	Time, location, and intensity of each historical TC record within the 800-km buffer of Hainan	China Meteorological Administration Tropical Cyclone Database (Lu et al., 2021; Ying et al., 2014)
Synthetic TC tracks	250 years	Time, location, and intensity of each synthetic TC record within the 800-km buffer of Hainan	Synthetic Tropical cyclOne geneRation Model Data set (STORM; Bloemendaal, De Moel, et al., 2020; Bloemendaal, Haigh, et al., 2020)
Land use	2020, 2018	Land uses including cropland, baer land, grassland, etc; Essential urban land uses including residential, commercial, industrial, transport, and public areas	GlobleLand30; Essential Urban Land Use Categories in China (EULUC-China; Gong et al., 2020)
Roads	2020	Polyline features with WGS84 coordinate system	Open Street Map
Populations	2020, 2100	Population distributions in 2020 (current) and 2100 (predicted for SSP1-1.9, SSP5-8.5), uniformed to a resolution of 100 m	WorldPop Gridded Population Count Data set (Bondarenko et al., 2020); Gridded data sets for population and economy under SSPs (Jiang et al., 2022)
Sea-level rise	2100	Local IPCC AR6 projections for the Haikou tidal gauge in 2100 (0.52 m for SSP1-1.9, and 0.91 m for SSP5-8.5)	IPCC 6th Assessment Report Sea Level Projections (Fox-Kemper et al., 2021; G. G. Garner, Kopp, et al., 2021; G. G. Garner, Hermans, et al., 2021)
Global flood damage database	2010	Economic exposure and flood depth-loss functions for agriculture, transport, commercial, industrial, and residential areas	European Commission Joint Research Center Publications Repository (Huizinga et al., 2017)

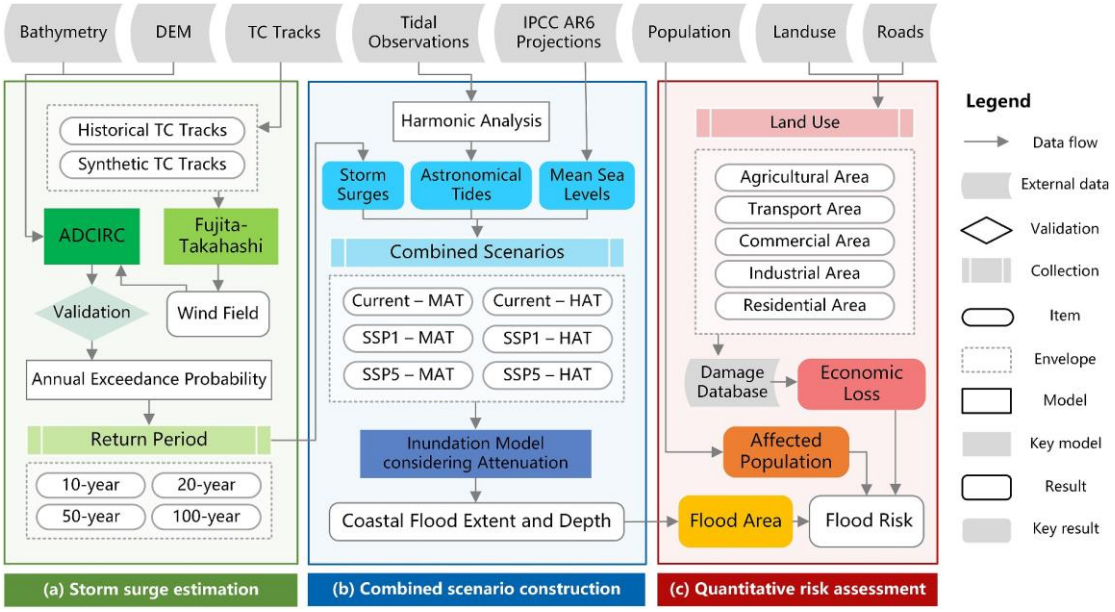

Fig 2 *Framework of the TCSoS-FRACS: (a) storm surge estimation; (b) combined scenario construction; and (c) quantitative risk assessment.*

water level was 5.65 cm with 80% of errors between -20 and 20 cm. Therefore, the ADCIRC model for Hainan Island is well-configured and suitable for subsequent study.

3.1.2 Estimation of Return Periods

Due to limited historical observations of TC tracks, it is challenging to fully assess TC-based storm surge risk, especially on a small scale (Bakker et al., 2022; Gori et al., 2020; Sridharan et al., 2022). Hence, we utilized synthetic TC tracks from the STORM (Synthetic Tropical cyclOne geneRation Model) data set for simulations. The STORM data set (Bloemendaal, Haigh, et al., 2020) extends global TC activities statistically over 10,000 years and can be used in various research domains (Almar et al., 2021; Bloemendaal, De Moel, et al., 2020; Meiler et al., 2022).

We conducted a series of preparatory procedures on the synthetic TC tracks from the STORM data set: (a) randomly selecting 250 years of TC activities from the data set to provide a robust estimation for storm surges at a 100-year return period (Dullaart et al., 2021; Hardy et al., 2004); (b) extracting the TC tracks that pass within a 200-km buffer of Hainan Island during the selected 250-year period (Lin et al., 2010; Qiu et al., 2022); (c) defining the potential impact distance as 800-km for each extracted track. This process resulted in 579 TC tracks, which were used to generate wind fields for input into the ADCIRC simulations. The resulting time series of water levels from ADCIRC for each mesh node included both astronomical tide and storm surge components. To isolate the storm surge component, we uniformly set the start time of the tidal force to 00:00 on 25 September 2020 and subtracted the astronomical tide from the total water levels.

Each synthetic TC track in the STORM data set includes corresponding year information. For each year within the selected 250-year period, we identified the annual maximum storm surge height at each mesh node based on this year information. These annual

maxima were then used to fit the Generalized Extreme Value (GEV) distribution to estimate the return levels of storm surge heights. The GEV fits demonstrated strong alignment with the annual maxima, with most R-squared values over 0.9 in Q-Q and P-P plots (details in Figure S7 in Supporting Information S1), which allowed us to accurately calculate the annual exceedance probabilities. Finally, we estimated storm surge heights for 10-, 20-, 50-, and 100-year return periods based on annual exceedance probabilities. Our uncertainty analysis revealed the 95% confidence interval for the 100-year return period was consistently within 0.2 m in most cases (details in Figure S8 in Supporting Information S1), underscoring the reliability and robustness of our estimates.

3.2 Combined Scenario Construction

Coastal water levels in this study were modeled by combining storm surges, astronomical tides, and mean sea levels. In the previous section, we generated storm surges at various return periods. Here, we forecasted local astronomical tides at mean and high levels using harmonic analysis and projected future local sea levels for SSP1- 1.9 and SSP5-8.5 scenarios in 2100. We then integrated these components to create combined scenarios for coastal flooding. Finally, we utilized a static inundation model considering water level attenuation to estimate flood extent and depth.

3.2.1 Astronomical Tides

Based on harmonic analysis (details in Text S3 in Supporting Information S1), tide levels were decomposed into tidal constituents with fixed periods (Passeri et al., 2016; Pringle et al., 2021). We used hourly observations from 12 tidal gauges along Hainan's coast (details in Table S2 in Supporting Information S1) for this analysis. Using the Matlab toolbox *S_TIDE* (Pan, 2023), we fitted amplitudes and phase lags of main tidal constituents to predict hourly tides for 2010–2030. The 10% exceedance probability was adopted as the high tide level (results in Table S3 in Supporting Information S1), aligning with the Chinese standard "Technical Regulations on the Risk of Marine Disasters in Large Coastal Projects" (Ministry of Natural Resources of the People's Republic of China, 2023). This metric includes frequent high tides and extreme events, allowing a comprehensive assessment of significant high tide impacts on coastal areas.

3.2.2 Mean Sea Levels

According to the IPCC AR6 report, global sea levels are projected to continue rising throughout the 21st century. Considering significant global variability in sea-level changes, we used projected values at the Haikou tidal gauge as a reference. By 2100, the local sea levels are estimated to rise by 0.52 m (SSP1-1.9) and 0.91 m (SSP5-8.5). Since the elevation data are referenced to the current sea level (0.07 m), we consider the relative sea-level rise values to be 0.45 m (SSP1-1.9) and 0.84 m (SSP5-8.5), respectively (Fox-Kemper et al., 2021; G. G. Garner, Kopp, et al., 2021; G. G. Garner, Hermans, et al., 2021).

3.2.3 Combined Scenario Settings

For ease of description, storm surges at 10-, 20-, 50-, and 100-year return periods were symbolized as RP010, RP020, RP050, and RP100; astronomical tides at mean and high

levels were symbolized as MAT and HAT; and mean sea levels at current and future scenarios (SSP1-1.9 and SSP5-8.5 in 2100) were symbolized as Current, SSP1, and SSP5. The combination of storm surges, astronomical tides, and mean sea levels theoretically resulted in 24 combined scenarios. For streamlined analysis, scenarios with the same astronomical tides and sea-level rise were grouped into 6 scenario sets: Current-MAT, Current-HAT, SSP1-MAT, SSP1-HAT, SSP5-MAT, and SSP5-HAT.

3.3 Quantitative Risk Assessment

Following the IPCC risk framework, we characterize coastal flooding as the interplay of hazard, exposure, and vulnerability. In the previous section, we estimated flood extent and depth under combined scenarios for the hazard dimension. This section integrates hazard with exposure and vulnerability, analyzing their collective impact on both economic losses and affected populations to provide a comprehensive quantification of risk. The risk for economic losses and affected populations are articulated through a unified equation:

$$R_X^S = H(s) \times \mathrm{E}(\mathrm{x}) \times \mathrm{V}(\mathrm{x})$$

where s denotes the flood scenario; x denotes the affected elements, either populations (p) or land use (l); Rs represents risk, quantified as either affected populations ($Rs\ p$) or economic losses ($Rs\ l$) for specific typical land use l; $H(s)$ represents hazard, measured by the flood area under scenario s; $E(x)$ represents exposure, measured by either population counts ($E(p)$) or unit maximum loss ($E(l)$) for specific land use l; $V(x)$ represents vulnerability, measured by a binary function $V(p)$ for populations (1 for flooded, 0 for non-flooded) or as the flood depth-loss function $V(l)$ for specific land use l.

For affected populations (R_{sp}), the population exposure ($E(p)$) encompasses both current and future levels. Current population data was sourced from WorldPop (Tatem, 2017) for the year of 2020 with a spatial resolution of 100 m. Future population projections were based on the work of Jiang et al. (2022), providing data for the year 2100 with a spatial resolution of 0.5°. To ensure consistency and enhance the spatial resolution of population exposure assessment, we calculated the growth rate for each grid from 2020 to 2100 and applied Inverse Distance Weighting (IDW) interpolation to downscale the coarse data to a 100-m resolution.

For economic losses (R_{sl}), the unit maximum loss ($E(l)$) (details in Table S4 in Supporting Information S1) and flood depth-loss functions ($V(l)$) (details in Figure S9 in Supporting Information S1) were both derived from the global flood damage database (Huizinga et al., 2017), which is designed for the typical land uses including agricultural, transport, commercial, industrial, and residential areas. Each land use type has corresponding unit maximum loss and flood depth-loss function. Due to the lack of specific classification for agricultural areas in the Essential Urban Land Use Categories (EULUC), we integrated agricultural areas from GlobeLand30 into a land use map. Furthermore, we supplemented the original EULUC with road data sourced from OpenStreetMap to address the transport areas (details in Table S5 in Supporting Information S1).

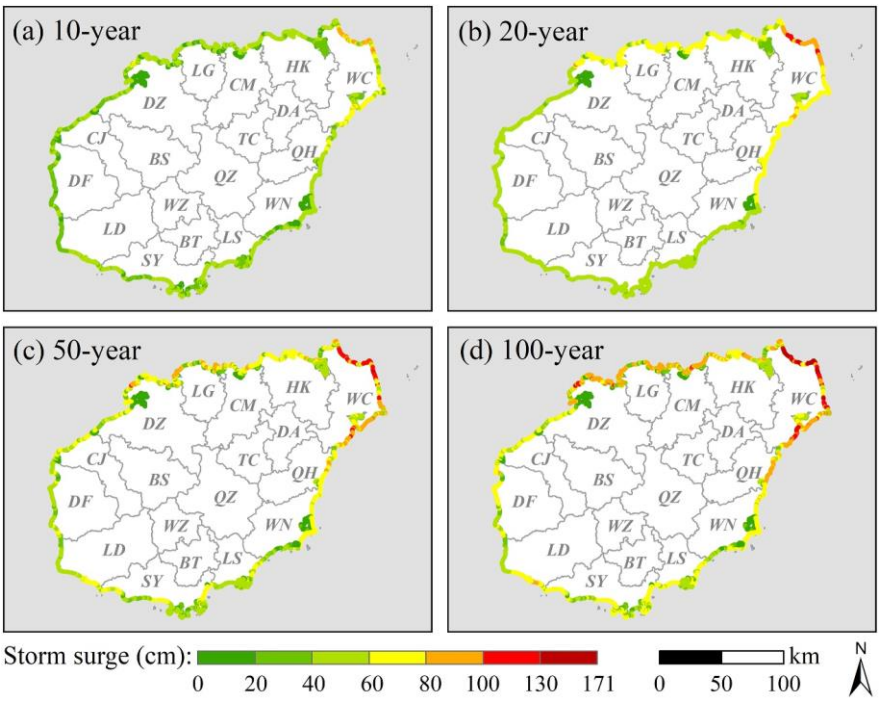

Fig 3 *Storm surges along the coast of Hainan Island for typical return periods: (a) 10-year return period; (b) 20-year return period; (c) 50-year return period; and (d) 100-year return period.*

4 Results

4.1 Storm Surges at Typical Return Periods

Based on simulation results along the coastline of Hainan Island, we have made a group of maps for storm surges at 10-, 20-, 50-, and 100-year return periods (RPs) (see Figure 3). It is evident that storm surges increase with higher RPs and exhibit a southwest-to-northeast upward trend spatially. Cities on the eastern side of Hainan Island, particularly Wenchang (WC), Qionghai (QH), and Wanning (WN), frequently experienced TC landfalls. Meanwhile, cities on the northern side, such as Haikou (HK), Chengmai (CM), Lingao (LG), and Danzhou (DZ), face a funnel effect with the opposite Leizhou Peninsula, causing seawater to accumulate in the Qiongzhou Strait.

Table 2 shows the statistical characteristics of storm surges, including proportions at different height levels, maximum values, and standard deviations. The maximum storm surge heights are 100 cm for the 10-year RP, 122 cm for the 20-year RP, 150 cm for the 50-year RP, and 171 cm for the 100-year RP. The standard deviation increases from 0.18 at 10-year RP to 0.29 at 100-year RP. These values are generally lower than previous results based on the extrapolation of historical tidal observations (Shi et al., 2019), with a maximum discrepancy of approximately 0.5 m at 100-year RP. Furthermore, only 0.01% of storm surges simulated along the coastline of Hainan Island exceed 1 m at the 10-year RP, increasing to 0.74% for the 20-year RP, 3.02% for the 50-year RP, and 5.31% for the 100-year RP. Additionally, the GEV fits for storm surges along the eastern coast reveal positive shape parameters (details in Figure S10 in Supporting Information S1), indicating

heavy-tailed characteristics. This suggests that extreme storm surges on eastern coast of Hainan Island may occur more frequently than anticipated by an exponential distribution.

Table 2

Statistical Characteristics of Storm Surges Along the Coastline of Hainan Island, Including Proportions at Different Height Levels, Maximum Values, and Standard Deviations

	Return period			
Storm surge (cm)	10-year	20-year	50-year	100-year
>100	0.01%	0.74%	3.02%	5.31%
>80	1.93%	3.36%	11.82%	24.63%
>60	7.93%	24.68%	43.87%	57.21%
>40	55.71%	65.70%	73.68%	76.63%
>20	81.58%	84.85%	87.39%	88.36%
Maximum	100	122	150	171
Standard deviation	0.18	0.21	0.25	0.29

4.2 Flood Under Combined Scenarios of High Tides and Sea-Level Rise

Figure 4 reveals the total flood area with depth contributions under combined scenarios. To assess the incremental hazard posed by combination of storm surges, high tides, and sea-level rise, we utilized the Current-MAT-RP010 scenario as a baseline. Under the scenario of RP100 storm surges with the same tide and sea-level conditions (Current-MAT-RP010), the total flood area is projected to be 1.80 times the baseline, with deeply flooded area (over 1 m) expanding to 5.74 times. For RP100 storm surges under high tide conditions (Current-HAT-RP100), the flood area could increase to 2.54 times, and deeply flooded area could expand to 16.24 times. Under combined conditions of high tides and sea-level rise (SSP1-HAT-RP100&SSP5-HAT-RP100), the flood area is expected to increase to 3.67–4.69 times, with deeply flooded area increasing to 30.19–44.93 times. These findings highlight the combined impact of various components on flooding, significantly exacerbating both the extent and depth of flood. Additionally, some coastal areas may be very sensitive to extreme flood hazards. To further explore the impact of high tides and sea-level rise on flooding, we analyzed RP100 storm surges across all scenarios. Transitioning from mean tides to high tides under current sea-level conditions (Current-MATRP100 to Current HAT-RP100) increased the flood area by 45.9 km^2. It becomes more pronounced under future sea-level conditions, with the SSP1-1.9 scenarios seeing a 59.3 km^2 increase (SSP1-MAT-RP100 to SSP1-HATRP100) and the SSP5-8.5 scenarios seeing a 68.0 km^2 increase (SSP5-MAT-RP100 to SSP5-HAT-RP100). This demonstrates that the effects of high tides are significantly amplified by sea-level rise. Similarly, transitioning from current to future sea level under mean tide conditions (Current-MAT-RP100 to SSP1-MAT-RP100 & SSP5- MAT-RP100) expanded the flood area by 57.5–111.2 km^2. Under high tide conditions, this expansion ranged from 70.9 to 133.2 km2 (Current-HAT-RP100 to SSP1-HAT-RP100 & SSP5- HAT-RP100),

underscoring how sea-level rise exacerbate flooding, with high tides further magnifying this effect.

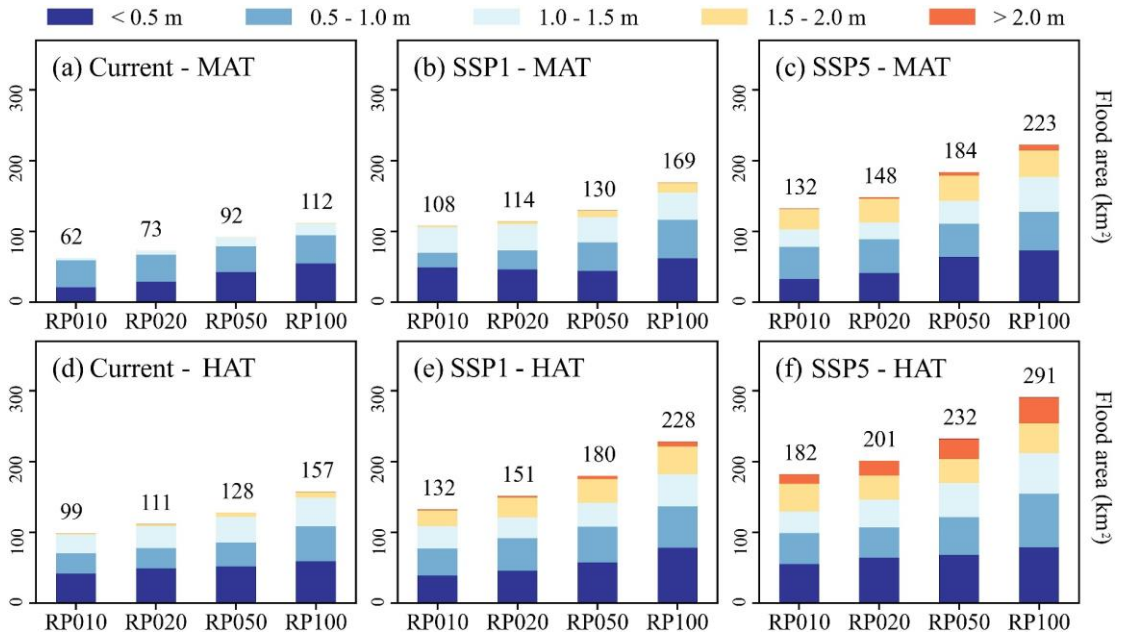

Fig 4 *Flood areas with depth contributions under combined scenarios: (a) scenario set Current-MAT; (b) scenario set SSP1-MAT; (c) scenario set SSP5-MAT; (d) scenario set Current-HAT; (e) scenario set SSP1-HAT; and (f) scenario set SSP5-HAT.*

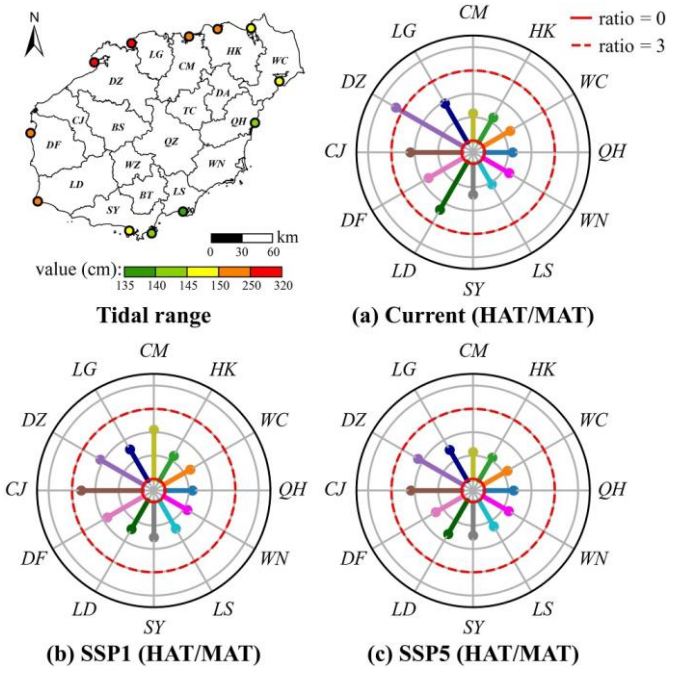

Fig 5 *Change ratios of flood area from mean tides to high tides for coastal cities on Hainan Island: (a) Current (HAT/MAT); (b) SSP1 (HAT/MAT); and (c) SSP5 (HAT/MAT). Subpanel (a) shows the change ratio of flood area from Current-MAT-RP100 to Current-HAT-RP100, with other subpanels following a similar pattern.*

Moreover, the lack of significant numerical differences between Current- HAT and SSP1-MAT scenarios, as well as SSP1-HAT and SSP5-MAT scenarios, raises interesting points

about the associated hazards with high tides and sea-level rise. This implies that current high tide conditions might already present hazards comparable to those expected from future sea-level conditions under the SSP1-1.9 scenario. Furthermore, the additional hazard induced by sea-level rise from the SSP1-1.9 to the SSP5-8.5 scenarios may be equivalent to that from mean tides to high tides in the future. This finding provides reassurance and confidence for climate change adaptation efforts. While the irreversible trend of sea-level rise driven by global warming poses significant threats to coastal areas, efforts for sustainable development, such as the use of clean energy, could mitigate the rising rate. Our study suggests that leveraging existing high tide flood management experience can inform the construction of defense measures against sea-level rise. To compare regional disparities in sensitivity to extreme flooding on Hainan Island, we generated a flood map for the worst-case scenario, SSP5-HATRP100 (Figure S11 in Supporting Information S1). Overall, flood hazards are higher in the northern regions and lower in the southern regions. The northern part features numerous narrow bays where seawater accumulates, making it susceptible to frequent TC impacts. In contrast, the southern part faces the South China Sea with open entrances and higher terrain, resulting in lower flood hazards. We have further analyzed five high-hazard areas in the central and northern parts of Hainan Island as follows: (a) coastal area from Haikou to Wenchang suffers the most severe flooding due to its flat terrain, allowing floodwaters to penetrate further inland; (b) coastal area of Dongfang has numerous narrow bays south of Changhua River, where flooding can exceed 2 m; (c) coastal area from Wanning to Qionghai is generally submerged by over 0.5 m, with flooding over 2 m near Boao Port; (d) coastal area from Danzhou to Lingao experiences significant tidal ranges, resulting in flooding over 3 m near Xinying Bay; (e) coastal area of Yinggehai is similarly affected by widespread flooding due to its flat topography. This analysis highlights the varying flood hazards across different regions of Hainan Island and underscores the need for targeted flood management strategies. To explore the relationship between tidal range and flood area, the spatial distribution of tidal ranges along the coastline of Hainan Island is shown in the top left corner of Figure 5. Visually, the tidal range is higher on the northwestern coast and lower in the southeastern coast, varying between 135 and 320 cm. The highest values are found near Danzhou (DZ) and Lingao (LG), while the lowest are near Lingshui (LS). Figure 5a illustrates the change ratios of flood area from mean tides to high tides under current sea-level conditions for each city, showing a high-west and low-east trend, with the greatest change in Danzhou (DZ), where the ratio exceeds 3. This indicates that, areas with greater tidal ranges experience more significant changes in flood area under current sealevel conditions, signifying the notable contribution of tidal range to flooding. Figure 5b demonstrates that under future low sea level (SSP1-1.9), spatial differences in flood area changes caused by tidal ranges diminish. Figure 5c further shows that under future high sea level (SSP5-8.5), sea-level rise further mitigates spatial differences in flood area caused by tidal ranges. These findings suggest that in the short term, high tides play a significant role in local coastal flooding, but in the long term, sea-level rise will become the dominant factor in future coastal flooding.

4.3 Risk Under Combined Scenarios of High Tides and Sea-Level Rise

Figure 6 illustrates the variations in flood area, economic losses and affected populations under combined scenarios. To quantify the incremental risk from the combination of storm surges, high tides, and sea-level rise, we benchmarked against the Current-MAT-RP010 scenario. Without considering high tides and sea-level rise, RP100 storm surges (Current-MAT-RP100) resulted in economic losses increasing to 1.70 times and affected populations to 1.60 times, indicating economic losses are more sensitive to storm surges than affected populations. Under high tide conditions, RP100 storm surges (Current-HAT-RP100) led to economic losses increasing to 2.57 times and affected populations to 2.26 times, highlighting the amplified disparity in sensitivity between economic losses and affected populations due to high tides. With both high tides and sea-level rise considered, RP100 storm surges (SSP1-HAT-RP100 & SSP5-HAT-RP100) caused economic losses to increase between 4.27–5.90 times and affected populations to increase between 4.96–6.23 times. Notably, the sensitivity of affected populations surpasses that of economic losses, suggesting severe sensitivity of affected populations to sea-level rise.

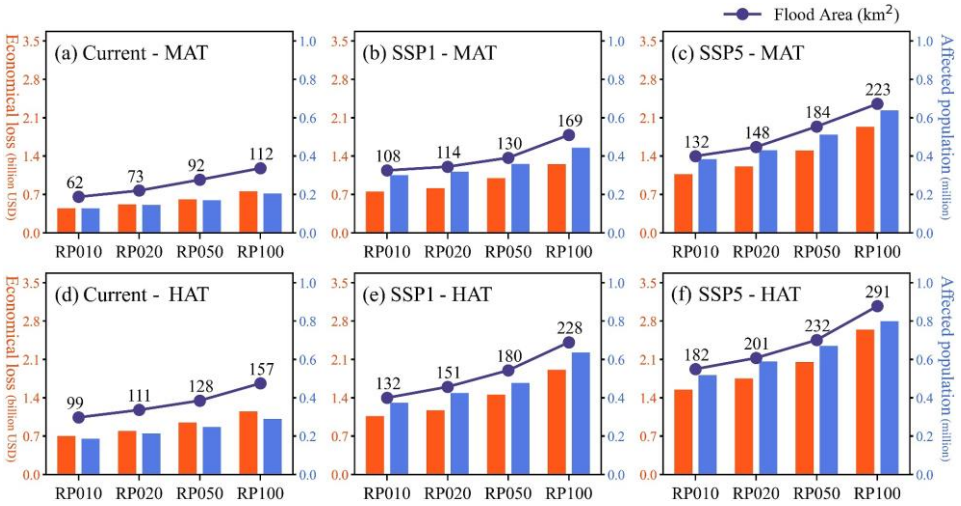

Fig 6 *Flood area, economic losses, and affected populations under combined scenarios: (a) scenario set Current-MAT; (b) scenario set SSP1-MAT; (c) scenario set SSP5-MAT; (d) scenario set Current-HAT; (e) scenario set SSP1-HAT; and (f) scenario set SSP5-HAT. Blue dotted lines represent flood area (km2), red bars represent economic loss (billion USD), and blue bars represent affected population (million).*

For a more in-depth analysis of the impacts of high tides and sea-level rise on risk, RP100 storm surges are applied across scenarios. Moving from mean tides to high tides under current sea-level conditions (Current-MAT-RP100 to Current-HAT-RP100) increased economic losses by 0.39 billion USD and affected populations by 0.09 million. Under future sea-level conditions, this increase becomes more significant: SSP1-1.9 scenarios led to a 0.66 billion USD increase in economic losses and a 0.19 million increase in affected populations (SSP1-MATRP100 to SSP1-HAT-RP100), while SSP5-8.5 scenarios led to a 0.71 billion USD increase in economic losses and a 0.16 million increase in affected populations (SSP5-MAT-RP100 to SSP5-HAT-RP100). This highlights the

significant amplification of risk due to high tides, further intensified by sea-level rise. Similarly, transitioning from current to future sea level under mean tide conditions (Current-MAT-RP100 to SSP1-MAT-RP100 & SSP5- MAT-RP100) expanded economic losses by 0.49–1.17 billion USD and affected populations by 0.24–0.43 million. Under high tide conditions, this expansion ranged from 0.76 to 1.49 billion USD for economic losses and from 0.35 to 0.51 million for affected populations (Current-HAT-RP100 to SSP1-HAT-RP100 & SSP5-HATRP100). These findings highlight the significant risk increase due to sea-level rise, which is further amplified under high tide conditions. Additionally, transitioning from the Fossil-fueled Development Pathway (SSP5-8.5 scenario) to the Sustainability Pathway (SSP1 - 1.9 scenario) could reduce the risk increase by approximately half.

To analyze flood risk disparities among cities under combined scenarios, we created a ring map of risk for 12 coastal cities on Hainan Island, covering maximum flood area, economic losses, and affected populations (see Figure 7). Haikou (HK) is classified as a "high hazard-high exposure" city, located on the northern coast. It faces multiple threats from storm surges, astronomical high tides, and TCs, leading to higher flood hazard. As the provincial capital, Haikou has a highly developed economy and large populations, resulting in higher exposure. In contrast, Sanya (SY) is a "low hazard-high exposure" city. Situated at the southernmost tip of the island and less susceptible to TC impacts, Sanya is the second-largest economic city, with significant populations and assets in low-lying coastal areas. Wenchang (WC) stands out as a "high hazard-low exposure" city, experiencing most frequent TC landfalls and extensive storm surge flooding. However, its high hazard zones do not spatially coincide with exposure, resulting in comparatively lower risk. It highlights that flood risk is not solely determined by flood area; it is a composite concept comprising hazard, exposure, and vulnerability.

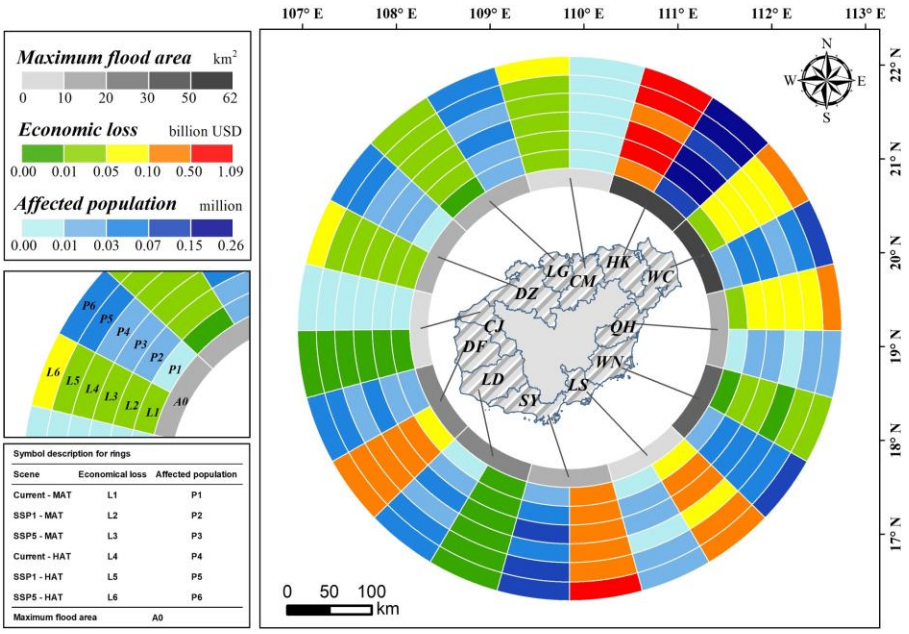

Fig 7 *Ring map of risk for coastal cities on Hainan Island, depicting maximum flood area, economic losses, and affected populations under combined scenarios.*

To further explore flood risk variations among coastal cities under combined scenarios, we focused on Haikou and Sanya, two cities with distinct risk profiles. Under the baseline scenario Current-MAT-RP100, Haikou incurred economic losses of 0.35 billion USD and affected populations of 0.08 million, while Sanya faced economic losses of 0.14 billion USD and affected populations of 0.03 million. Under high tide conditions (Current-HAT-RP100), economic losses increased to 1.44 times in Haikou and 1.41 times in Sanya; affected populations increased to 1.33 and 1.17 times, respectively. Under combined conditions of high tides and sea-level rise (SSP1-HAT-RP100 & SSP5-HAT-RP100), the amplifying effect was even more pronounced: economic losses escalated to 2.39–3.15 times in Haikou and 2.62–3.98 times in Sanya; affected populations increased to 2.85–3.34 times and 3.96–5.26 times, respectively. Experience from Sanya demonstrates that low-hazard areas do not necessarily imply low risk, especially where populations and assets are highly exposed. These areas may experience a dramatic escalation of coastal flood risk under high tides and sea-level rise, necessitating vigilance in future urban planning.

A set of risk curves for economic losses (based on typical land uses) and affected populations was developed to investigate how flood risk changes under combined scenarios (see Figure 8). Here, the return periods of storm surges are characterized as hazard probabilities: RP010 (0.1), RP020 (0.05), RP050 (0.02), and RP100 (0.01). For economic losses, risk for different land uses are ranked from high to low as follows: residential area, industrial area, commercial area, transport area, and agricultural area. The high risk for residential and industrial areas is due to their large spatial coverage, occupying areas of 324.41 and 211.54 km2 respectively, and their high unit loss values, with 66 USD·$^{m-2}$ and 127 USD·m^{-2} respectively. Regarding each land use, the Current-MAT scenario set exhibits the lowest risk, while the SSP5-HAT scenario set presents the highest risk. Notably, the risk curves for SSP5-MAT and SSP1-HAT, as well as SSP1-MAT and Current-HAT, show partial overlaps, indicating a similarity in the response of risk to both high tides and sea-level rise during certain periods. For the affected populations, risk under six combined scenario sets are ranked from low to high as follows: Current-MAT, Current- HAT, SSP1-MAT, SSP1-HAT, SSP5-MAT, and SSP5-HAT. Similar to flood hazards, the impacts of sea-level rise on populations are higher than that of high tides.

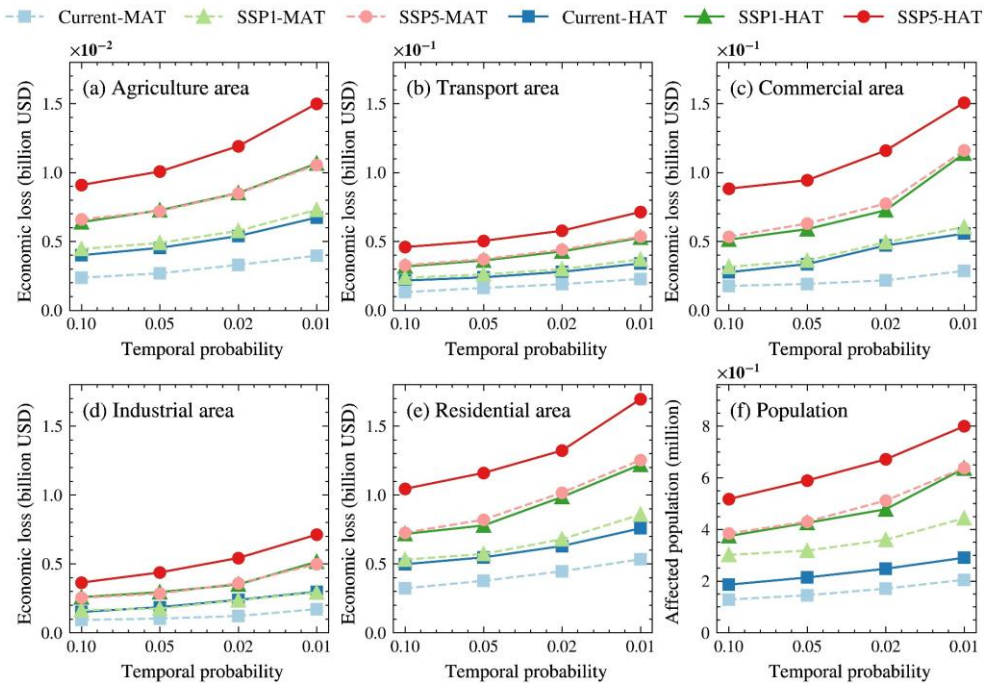

Fig 8 *Risk curves for economic losses (based on typical land uses) and affected populations under combined scenarios. (a) agriculture area; (b) transport area; (c) commercial area; (d) industrial area; (e) residential area; and (f) population. The y-axes of subpanels (a), (b), (c), and (f) are in scientific notation to accommodate the varying scales of economic losses and affected populations. The notation "10 1" indicates values should be multiplied by 0.1, while "10 2" indicates values should be multiplied by 0.01.*

5 Discussion

5.1 Comparisons With Related Studies

Most previous studies on storm surges in Hainan Island have relied on statistical analyses of historical observations (Fang et al., 2021; Gao et al., 2014; Shi et al., 2019). These studies, limited by sparse observation coverage and short-term records, often led to significant biases and substantial uncertainties when extrapolating for extreme events. For instance, our study finds that previous statistical estimations of storm surges along Hainan Island are generally higher than our results (Shi et al., 2019), with a maximum discrepancy of approximately 0.5 m at 100- year RP. The advent of the STORM data set (Bloemendaal, Haigh, et al., 2020; Bloemendaal et al., 2022), which extends global TC activities over 10,000 years, addresses the limitation of insufficient historical TC data on a local scale. In this context, Wood et al. (2023) set a precedent by simulating storm surges in the South China Sea using the STORM data sets. Our study refines this work by improving the resolution along the coast of Hainan Island from 5 km to 400 m, allowing for more detailed flood information at bays and estuaries.

Traditional Chinese risk assessments for storm surges, particularly in regions with underdeveloped economic and observational capabilities, often rely on an indicator-based approach. This approach, exemplified by the current Chinese industry standard "Technical Directives for Risk Assessment and Zoning of Marine Disaster" (Ministry of

Natural Resources of the People's Republic of China, 2019), uses a series of standardized indicators to represent key risk components, aggregated through weighted summation or multiplication for overall risk assessment. While straightforward and easy to implement, it offers only a relative risk magnitude, constrained by data accuracy and subjective interpretations. In contrast, our study created a series of detailed risk curves for economic losses and affected populations across various scenarios, integrating hazard, exposure, and vulnerability. This approach not only quantifies loss values precisely but also anticipates loss variations with changing storm surge levels. It advances our comprehension of risk impacts, guiding risk assessments beyond Hainan Island and enabling government agencies to formulate informed response and risk management strategies.

5.2 New Insights and Implications

Our study found that coastal flooding on Hainan Island is approximately equivalent between the Current-HAT and SSP1-MAT scenarios. This suggests that hazards from future sea-level rise under a sustainable scenario may be comparable to those from current high tides, providing reassurance and confidence for climate change adaptation efforts. Sea-level rise due to global warming is an unavoidable challenge with deep uncertainty (A. J. Garner et al., 2023; Kopp et al., 2014, 2023). Our study examines two future scenarios for climate change: SSP1- 1.9 (Sustainable Development Pathway) and SSP5 - 8.5 (Fossil - fueled Development Pathway). The former emphasizes balancing economic growth with environmental protection, focusing on social equity and efficient resource use, while the latter prioritizes rapid economic growth, potentially leading to resource depletion, environmental degradation, and social instability in the long term (O' Neill et al., 2014, 2016). As the saying goes, "Pessimists are usually right and optimists are usually wrong, but all the great changes have been accomplished by optimists." While some studies focus on worst-case scenarios and highlight the catastrophic consequences of extreme events (Qiu et al., 2022; Yin et al., 2021), these can undermine public and government confidence, leading to panic and resignation (Moser & Dilling, 2011). Although sea-level rise is an irreversible trend, global cooperation in promoting clean energy and green economic development can slow the rate of change. Our study suggests that drawing on existing high tide flood management experience can inform the construction of defense measures against sea-level rise.

Our projections indicate that from the Current-MAT scenario to the SSP1-HAT and SSP5-HAT scenarios, Sanya's economic losses will increase to 2.62–3.98 times, and affected populations will increase to 3.96–5.26 times. Experience from Sanya highlights the need for heightened vigilance regarding future flood risk in coastal cities currently classified as "low hazard-high exposure." Haikou and Sanya represent "high hazard-high exposure" and "low hazard - high exposure" among the coastal cities of Hainan, respectively. Traditionally, flood defense infrastructure is designed based on the return period of historical coastal water levels (Serafin et al., 2024), which corresponds to hazard levels. Consequently, Haikou, characterized by "high hazard," typically receives more attention and resources for the construction and maintenance of defense infrastructure. In contrast,

Sanya, classified as “low hazard,” is often overlooked. This neglect can be reflected in the flood defense standards, with Haikou's standards set for 50–100 years RP events, while Sanya's standards are set for 20–50 years RP events (People's Government of Hainan Province, 2015). This is detrimental for Sanya, as extreme flood events exceeding the defense standards can have devastating consequences for high-exposure coastal areas. Research has shown that the South China Sea region frequently faces flood events triggered by astronomical tides alone (S. Li et al., 2023). Additionally, as the local sea level continues to rise, the freeboard between high water levels and local flood thresholds will further decrease (Ghanbari et al., 2019). Combined with the rapid urbanization and concentration of economic activities and populations in low-lying areas, this could lead to a sharp increase in future flood risk.

5.3 Adaptability to Other Regions

The selection of Hainan Island for our study is motivated by its strategic position as China's free trade port linking Southeast and South Asia, and its potential implications for other regions with similar geographical environments and risk profiles. This makes our findings potentially catalytic in enhancing coastal community resilience and reducing disaster risk in these regions. Small Island Developing States (SIDS) share many similarities with Hainan Island. Precious yet limited land space is crucial for supporting rapid population growth and urban expansion (Umeyama, 2012). Especially in low-lying coastal areas, lower construction costs and cheaper transportation attract industries and concentrated populations (Mycoo et al., 2021). Unfortunately, despite their low carbon emissions, these regions bear disproportionate destructive consequences of global climate change. Studies show that sea-level rise causes over 6% of SIDS areas to flood annually (Vousdoukas et al., 2023), and SIDS constitute more than 60% of the countries suffering the highest losses from coastal disasters, with over 9% of their GDP (Giardino et al., 2018). The lack of resource diversity and inappropriate land use further exacerbate risk sensitivity.

The TCSoS-FRACS model can be adapted for other specific islands or regions with unique geographical and socio-economic characteristics. By inputting new parameters relevant to a specific location, such as updated bathymetry, digital elevation models, and socio-economic data, the model can generate unique results tailored to those regions. Local governments can optimize resource allocation and infrastructure construction based on the assessment results. For example, in planning new urban development areas, model-predicted flood risk can inform safer site selections. In flood control engineering, data from the model can prioritize strengthening defenses in high-risk areas rather than just high-hazard areas. In conclusion, the model constructed and insights gained from our study on Hainan Island can be effectively applied to SIDS, providing a valuable framework for risk management and disaster mitigation.

5.4 Limitations

Several limitations remain in this study: (a) While the static risk assessment intuitively identifies high-risk areas and supports rapid scientific decision-making, it overlooks the

actual evolution process of floods and therefore cannot provide dynamic risk alerts. (b) The estimation of economic losses is based on the current land use patterns, disregarding potential future changes. Policies play a pivotal role in altering land use, especially in China (Liu et al., 2014; J. Wang, Lin, et al., 2018), and predicting these changes remains a significant challenge. (c) The construction of combined scenarios did not account for the nonlinear interactions among storm surges, astronomical tides, and sea-level rise (Bilskie et al., 2022; Serafin, Ruggiero, Barnard, & Stockdon, 2019), due to the associated deep uncertainties. These issues deserve further attention and discussion in future studies.

6 Conclusion

In this study, we developed a comprehensive quantitative risk framework, TCSoS-FRACS, designed to assess storm surge risk under combined scenarios of high tides and sea-level rise. By integrating dynamic and statistical models, TCSoS-FRACS strikes a balance between reliability and efficiency, enhancing the accuracy of risk assessments and their applicability to diverse settings. Unlike traditional assessments that primarily focus on hazards, our study elucidates three critical components of risk: hazard, exposure, and vulnerability. This model incorporates economic and demographic factors, providing a deeper understanding of risk composition and serving as a versatile tool for disaster risk management.

The distinctive contribution of our study lies not only in its holistic approach to assessing storm surge flood risk, but also in its application to Hainan Island with broad implications. Our findings indicate that the combined impact of storm surges, high tides, and sea-level rise will significantly increase future coastal flood risk on Hainan Island. Specifically, from Current-MAT-RP010 to SSP1-HAT-RP100 and SSP5-HAT-RP100 scenarios, economic losses are projected to increase to 4.27–5.90 times, and affected populations to 4.96–6.23 times. Moreover, transitioning from the Fossil-fueled Development Pathway (SSP5-8.5) to the Sustainability Pathway (SSP1-1.9) could reduce the risk increase by approximately half. The equivalence of flood risk between current high tides and future sea level under a sustainable scenario bolsters confidence in adaptation efforts. However, coastal cities with low hazard but high exposure need heightened vigilance in flood defense, as future risk could escalate sharply.

Our results provide valuable scientific guidance for Hainan Island and other regions with similar risk profiles. These regions can leverage our findings to enhance resilience and disaster mitigation strategies. Additionally, the development of this model aids in the effective allocation of disaster relief resources, optimization of reconstruction investments, and provision of critical benchmarks for the insurance industry, supporting an integrated approach to disaster risk management. This comprehensive assessment technique demonstrates how integrated evaluations can promote more effective policy-making and urban planning, offering valuable references for regions facing similar threats.

7 Data Availability Statement

All input data used in this study are open-source and listed in Table 1 from Section 2.2. Historical tidal observations are available from the China Marine Data Center (https://mds.nmdis.org.cn/pages/tidalCurrent.html). Land use data is sourced from GlobleLand30 (https://www.webmap.cn/mapDataAction.do?method-=globalLandCover), and road data is available from Open Street Map (http://www.openstreetmap.org/). The ADCIRC model (V53) can be obtained from its official website (https://adcirc.org/). All source code and processed data for the TCSoS-FRACS model are publicly available on GitHub (https://github.com/Neptunie99/TCSoS-FRACS) and preserved as a repository on Zenodo (Zhou et al., 2024).

8 References

Almar, R., Ranasinghe, R., Bergsma, E. W. J., Diaz, H., Melet, A., Papa, F., et al. (2021). A global analysis of extreme coastal water levels with
implications for potential coastal overtopping. Nature Communications, 12(1), 3775. https://doi.org/10.1038/s41467 - 021 - 24008 - 9

Anderson, D. L., Ruggiero, P., Mendez, F. J., Barnard, P. L., Erikson, L. H., O’ Neill, A. C., et al. (2021). Projecting climate dependent coastal
flood risk with a hybrid statistical dynamical model. Earth's Future, 9(12), e2021EF002285. https://doi.org/10.1029/2021EF002285

Bakker, T. M., Antolinez, J. A. A., Leijnse, T. W. B., Pearson, S. G., & Giardino, A. (2022). Estimating tropical cyclone - induced wind, waves, and
surge: A general methodology based on representative tracks. Coastal Engineering, 176, 104154. https://doi.org/10.1016/j.coastaleng.2022.
104154

Bilskie, M. V., Angel, D. D., Yoskowitz, D., & Hagen, S. C. (2022). Future flood risk exacerbated by the dynamic impacts of sea level rise along
the Northern Gulf of Mexico. Earth's Future, 10(4), e2021EF002414. https://doi.org/10.1029/2021EF002414

Bloemendaal, N., De Moel, H., Martinez, A. B., Muis, S., Haigh, I. D., van der Wiel, K., et al. (2022). A globally consistent local - scale assessment
of future tropical cyclone risk. Science Advances, 8(17), eabm8438. https://doi.org/10.1126/sciadv.abm8438

Bloemendaal, N., De Moel, H., Muis, S., Haigh, I. D., & Aerts, J. C. J. H. (2020). Estimation of global tropical cyclone wind speed probabilities
using the STORM dataset. Scientific Data, 7(1), 377. https://doi.org/10.1038/s41597 - 020 - 00720 - x

Bloemendaal, N., Haigh, I. D., De Moel, H., Muis, S., Haarsma, R. J., & Aerts, J. C. J. H. (2020). Generation of a global synthetic tropical cyclone
hazard dataset using STORM [Dataset]. Scientific Data, 7(1), 40. https://doi.org/10.1038/s41597 - 020 - 0381 - 2

Bondarenko, M., Kerr, D., Sorichetta, A., & Tatem, A. (2020). Census/projection - disaggregated gridded population datasets for 189 countries in
2020 using Built - Settlement Growth Model (BSGM) outputs [Dataset]. University of Southampton. https://doi.org/10.5258/SOTON/WP00684
Bruneau, N., Polton, J., Williams, J., & Holt, J. (2020). Estimation of global coastal sea level extremes using neural networks. Environmental
Research Letters, 15(7), 074030. https://doi.org/10.1088/1748 - 9326/ab89d6
Calafat, F. M., Wahl, T., Tadesse, M. G., & Sparrow, S. N. (2022). Trends in Europe storm surge extremes match the rate of sea - level rise. Nature,
603(7903), 841 – 845. https://doi.org/10.1038/s41586 - 022 - 04426 - 5
Camus, P., Haigh, I. D., Nasr, A. A., Wahl, T., Darby, S. E., & Nicholls, R. J. (2021). Regional analysis of multivariate compound coastal flooding
potential around Europe and environs: Sensitivity analysis and spatial patterns. Natural Hazards and Earth System Sciences, 21(7), 2021 – 2040.
https://doi.org/10.5194/nhess - 21 - 2021 - 2021
Camus, P., Losada, I. J., Izaguirre, C., Espejo, A., Menendez, M., & Perez, J. (2017). Statistical wave climate projections for coastal impact
assessments: Statistical wave climate projections. Earth's Future, 5(9), 918 – 933. https://doi.org/10.1002/2017EF000609
Castrucci, L., & Tahvildari, N. (2018). Modeling the impacts of sea level rise on storm surge inundation in flood - prone urban areas of Hampton
Roads, Virginia. Marine Technology Society Journal, 52(2), 92 – 105. https://doi.org/10.4031/MTSJ.52.2.11
Dullaart, J. C. M., Muis, S., Bloemendaal, N., Chertova, M. V., Couasnon, A., & Aerts, J. C. J. H. (2021). Accounting for tropical cyclones more
than doubles the global population exposed to low - probability coastal flooding. Communications Earth & Environment, 2(1), 135. https://doi.
org/10.1038/s43247 - 021 - 00204 - 9
Edmonds, D. A., Caldwell, R. L., Brondizio, E. S., &Siani, S. M. O. (2020). Coastal flooding will disproportionately impact people on river deltas.
Nature Communications, 11(1), 4741. https://doi.org/10.1038/s41467 - 020 - 18531 - 4
Eilander, D., Couasnon, A., Sperna Weiland, F. C., Ligtvoet, W., Bouwman, A., Winsemius, H. C., & Ward, P. J. (2023). Modeling compound
flood risk and risk reduction using a globally applicable framework: A pilot in the Sofala province of Mozambique. Natural Hazards and Earth
System Sciences, 23(6), 2251 – 2272. https://doi.org/10.5194/nhess - 23 - 2251 - 2023
Fang, J., Sun, S., Shi, P., & Wang, J. (2014). Assessment and mapping of potential storm surge impacts on global population and economy.
International Journal of Disaster Risk Science, 5(4), 323 – 331. https://doi.org/10.1007/s13753 - 014 - 0035 - 0
Fang, J., Wahl, T., Fang, J., Sun, X., Kong, F., & Liu, M. (2021). Compound flood potential from storm surge and heavy precipitation in coastal

China: Dependence, drivers, and impacts. Hydrology and Earth System Sciences, 25(8), 4403 – 4416. https://doi.org/10.5194/hess - 25 - 4403 -
2021
Fox - Kemper, B., Hewitt, H. T., Xiao, C., Adalgeirsdottir, G., Drijfhout, S. S., Edwards, T. L., et al. (2021). Ocean, cryosphere and sea level
change. In Climate Change 2021: The Physical Science Basis. In Contribution of Working Group I to the Sixth Assessment Report of the
Intergovernmental Panel on Climate Change (pp. 1211 – 1362). Cambridge University Press.
Fujita, T. (1952). Pressure distribution within typhoon. Geophysical Magazine, 23, 437 – 451.
Gao, Y., Wang, H., Liu, G. M., Sun, X. Y., Fei, X. Y., Wang, P. T., et al. (2014). Risk assessment of tropical storm surges for coastal regions of
China. Journal of Geophysical Research: Atmospheres, 119(9), 5364 – 5374. https://doi.org/10.1002/2013jd021268
Garner, A. J., Sosa, S. E., Tan, F., Tan, C. W. J., Garner, G. G., & Horton, B. P. (2023). Evaluating knowledge gaps in sea - level rise assessments
from the United States. Earth's Future, 11(2), e2022EF003187. https://doi.org/10.1029/2022EF003187
Garner, G. G., Hermans, T., Kopp, R. E., Slangen, A. B. A., Edwards, T. L., Levermann, A., et al. (2021). IPCC AR6 sea - level rise projections,
version 20210809. PO. DAAC. Retrieved from https://podaac.jpl.nasa.gov/announcements/2021 - 08 - 09 - Sea - level - projections - from - the - IPCC -
6th - Assessment - Report
Garner, G. G., Kopp, R. E., Hermans, T., Jha, S., Kumar, P., Reedy, A., et al. (2021). Framework for assessing changes to sea - level (FACTS).
Geoscientific Model Development, 16(24), 7461 – 7489. https://doi.org/10.5194/gmd - 16 - 7461 - 2023
Ghanbari, M., Arabi, M., Obeysekera, J., & Sweet, W. (2019). A coherent statistical model for coastal flood frequency analysis under nonstationary
sea level conditions. Earth's Future, 7(2), 162 – 177. https://doi.org/10.1029/2018EF001089

Indications of contributions to Global Risk Research Framework and UN Agendas[1]

1. How does this study contribute to Global Risk Research Framework Priorities?

The study examines the complex interplay between storm surges, high tides, and sea-level rise. It highlights how these factors, when combined, exacerbate flood risks, creating systemic vulnerabilities (Research Priority 1). The study contributes to global risk research by presenting a comprehensive flood risk assessment framework (TCSoS-FRACS) which integrates storm surges, high tides, and sea-level rise to address the challenges of assessing coastal flood risks under climate change. This challenges traditional, single-dimensional hazard assessments by providing a multidimensional understanding of how these factors interact under different climate scenarios (Research Priority 4). By combining advanced statistical models, dynamic simulations (e.g., ADCIRC model), and extensive datasets (e.g., synthetic tropical cyclone tracks and IPCC sea-level rise projections), the study demonstrates innovative methods for accurately quantifying and mapping flood risks. This approach enhances predictive capabilities and provides actionable insights for disaster risk management and adaptation planning (Research Priority 5).

2. How does this study contribute to SFDRR targets?

The study supports SFDRR targets in several aspects. Promoting understanding of disaster risk through quantitative assessments of combined hazards, exposure, and vulnerability. Strengthening disaster risk governance by offering a versatile tool for policymakers to enhance decision-making. Facilitating in disaster risk reduction through actionable strategies that can guide coastal defense enhancements. Boosting disaster preparedness by highlighting the need for adaptive measures against future risks intensified by sea-level rise and high tides.

3. How does this study contribute to SDGs?

The study is closely related to Sustainable Development Goal target 13 (Climate Action), especially its target 13.1: strengthen resilience and adaptive capacity to climate-related hazards and natural disasters in all countries; SDG target 13.3: Improve education, awareness-raising and human and institutional capacity on climate change mitigation, adaptation, impact reduction and early warning. SDG target 11 (Sustainable Cities and Communities), especially target 11.5: By 2030, significantly reduce the number of deaths

[1] This section was drafted by IRDR IPO team.

and the number of people affected and substantially decrease the direct economic losses relative to global gross domestic product caused by disasters, including water-related disasters, with a focus on protecting the poor and people in vulnerable situations.

4. How does this study contribute to Paris Agreement?

The study aligns with the Paris Agreement by:

Showcasing the effectiveness of transitioning from a fossil-fueled development pathway (SSP5-8.5) to a sustainability pathway (SSP1-1.9), which can halve flood risk increases.

Supporting adaptation strategies that enhance resilience to climate impacts, consistent with the Agreement's goals of fostering climate-resilient development.

Providing confidence in current and future adaptation efforts through evidence-based hazard equivalency analysis between current high tides and future sea-level rise.